Flux qubit interaction with rapid single-flux quantum logic circuits: Control and readout

N. V. Klenov, A. V. Kuznetsov, I. I. Soloviev, S. V. Bakurskiy, M. V. Denisenko, and A. M. Satanin

Citation: Low Temperature Physics **43**, 789 (2017); doi: 10.1063/1.4995627
View online: http://dx.doi.org/10.1063/1.4995627
View Table of Contents: http://aip.scitation.org/toc/ltp/43/7
Published by the American Institute of Physics

Flux qubit interaction with rapid single-flux quantum logic circuits: Control and readout

N. V. Klenov[a)]

Physics Faculty, Lomonosov Moscow State University, 1 Leninskiye Gory, Building 2, Moscow 119991, Russia; Skobeltsyn Institute of Nuclear Physics, Lomonosov Moscow State University, 1 Leninskiye Gory, Building 2, Moscow 119991, Russia; Moscow Technical University of Communications and Informatics, 8a Aviamotornaya St., Moscow 111024, Russia; and Moscow Institute of Physics and Technology, State University, 9 Institutskiy Ave., Dolgoprudny, Moscow 141700, Russia

A. V. Kuznetsov

Physics Faculty, Lomonosov Moscow State University, 1 Leninskiye Gory, Building 2, Moscow 119991, Russia

I. I. Soloviev and S. V. Bakurskiy

Skobeltsyn Institute of Nuclear Physics, Lomonosov Moscow State University, 1 Leninskiye Gory, Building 2, Moscow 119991, Russia and Moscow Institute of Physics and Technology, State University, 9 Institutskiy Ave., Dolgoprudny, Moscow 141700, Russia

M. V. Denisenko and A. M. Satanin

Lobachevsky State University of Nizhny Novgorod, 23 Gagarina Ave., Nizhniy Novgorod, Nizhegorodskaya 603022, Russia

(Submitted February 1, 2017)
Fiz. Nizk. Temp. **43**, 991–1002 (July 2017)

We present the results of an analytical study and numerical simulation of the dynamics of a superconducting three-Josephson-junction (3JJ) flux qubit magnetically coupled with rapid single-flux quantum (RSFQ) logic circuit, which demonstrate the fundamental possibility of implementing the simplest logic operations at picosecond times, as well as rapid non-destructive readout. It is shown that when solving optimization problems, the qubit dynamics can be conveniently interpreted as a precession of the magnetic moment vector around the direction of the magnetic field. In this case, the role of magnetic field components is played by combinations of the Hamiltonian matrix elements, and the role of the magnetic moment is played by the Bloch vector. Features of the 3JJ qubit model are discussed during the analysis of how the qubit is affected by exposure to a short control pulse, as are the similarities between the Bloch and Landau-Lifshitz-Gilbert equations. An analysis of solutions to the Bloch equations made it possible to develop recommendations for the use of readout RSFQ circuits in implementing an optimal interface between the classical and quantum parts of the computer system, as well as to justify the use of single-quantum logic in order to control superconducting quantum circuits on a chip. *Published by AIP Publishing.*
[http://dx.doi.org/10.1063/1.4995627]

1. Introduction

Modern experimental studies on superconducting qubits require precise control over their states while simultaneously minimizing the inverse effects of readout and control circuits on quantum circuits. One of the most promising ideas in this arena has been the attempt to combine qubits with classical lines of rapid single-flux quantum (RSFQ) logic circuits.[1–9] The use of such cryogenic digital electronics can provide a more reliable method of controlling the quantum circuits on a chip, than control and readout using EM control pulses sent over coaxial cables. A serious drawback of traditional RSFQ circuits is the use of shunted Josephson junctions that introduce energy dissipation to quantum computing systems. Minimizing the contribution of control RSFQ circuits to the decoherence processes in quantum register states is an important part of developing the optimal interface between the classical and the quantum parts of a computer.

The very first experiments with flux qubits used a non-shunted superconducting quantum interference device (SQUID) for state readout; the device changed to a resistive state with one direction of the circular current in the qubit and remained in the superconducting state at the other, when a current pulse was applied. An analogue of this readout method could be the use of one of the more common elements of the RSFQ library, which is a balanced comparator. Depending on the ratio between the current induced by the qubit magnetic flux and the reference current, when the readout pulse arrives at the balanced comparator input, a single-flux quantum (SFQ) pulse can be formed at the output of the circuit, symbolizing the logic unit in RSFQ circuits (the absence of a single-flux quantum pulse per clock period denotes a logic zero).

A successful example of applying interface RSFQ circuits to the study of quantum systems is Ref. 2, in which the classical circuits were used to control the state of one type of flux qubit, known as the vortex qubit. A RSFQ converter of the analog signal into the single-flux quantum pulse, also known as a DC/SFQ converter, was used to initialize the system, which involves the entry of a Josephson vortex into a long Josephson junction. A so-called RS flip-flop, which changes its state when a magnetic flux quantum Φ_0 appears at its input, is connected to the other end of the long Josephson junction for qubit state readout.

In order to implement a weakly perturbing readout of the qubit states using RSFQ circuits[2–9] the use of SFQ pulses (fluxons) and Josephson transmission lines (JTL) was proposed, based on long non-shunted transitions. Due to the weak magnetic coupling with the flux qubit, effective potential arises across the JTL, which spreads the propagating ballistic fluxon. The qubit state in such a circuit determines the change in fluxon propagation time from the generator (G) to the "SFQ Detector," which is measured using a comparison circuit with a reference line (using comparator C).

Further optimization of this concept[10] by way of detector circuit symmetrization allowed for further significant reductions in the inverse effect the readout process has on the qubit due to the magnetic coupling of the qubits with both detector JTLs, such that the fluxons at each shoulder are scattered on induced current inhomogeneities [Fig. 1(a)]. With this type of coupling the inverse effect on the qubit is determined by the accumulated time delay between fluxons, and not by the size of the JTL segment coupled with the qubit. With the parameters chosen in Ref. 10, the pulse area that is dependent on the time of the effective magnetic flux turns out to be an order of magnitude smaller for the symmetrized circuit [Fig. 1(b)], as opposed to the original circuit proposed in Ref. 3.

It is important to emphasize that the described approach can also be used for traditional RSFQ circuits based on discrete JTLs, which are a parallel junction of non-shunted or weakly shunted contacts, as well as for simultaneous readout of N qubit states. To do this, after exiting the single-flux quantum pulse generator a fluxon must pass through a splitter tree, at the output of which $2N$ of such single-flux quantum pulses are simultaneously assigned to the described interferometric detection circuits [Fig. 1(a)].

The task before this article is to analyze the dynamics of the Josephson qubits over the course of such readout procedures. In addition, we plan to demonstrate that under certain conditions the interaction of an artificial atom and the JTL can be used to generate controllable changes to its state at picosecond times.[11–13]

2. The dynamics of the Josephson qubit state during fluxon interaction

2.1. Readout and control: selecting the fluxon exposure parameters

Let us begin our discussion on the dynamic behavior of a superconducting flux qubit in an alternating magnetic field from the simplest two-level approximation, when the particular type of qubit is not specified[14]

$$H(t) = \frac{1}{2}(\Delta\sigma_z + \varepsilon(t)\sigma_x), \tag{1}$$

where the time independent distance between the qubit levels Δ is coupled with the transition frequency between levels $\omega_{01} = (E_1 - E_0)\hbar$ (excited "1" with energy E_1 and ground "0" with energy E_0). In turn, the control function $\varepsilon(t)$ is related to amplitude A and envelope $f(t)$ by the relation $\varepsilon(t) = 2Af(t)$.

Within the framework of our concept[13] we propose that it is through the minor diagonal matrix elements of the Hamiltonian that the effects of the external "unipolar" magnetic field on the state of the qubit are manifested, and that the characteristics of this magnetic field are the envelope and the amplitude. We associate this effect with the wave of currents propagating across the JTL coupled with the qubit during fluxon motion. The most characteristic [see Fig. 1(b)] shape of the envelope $f(t)$ of the pulsed unipolar field is the continuous Heaviside function with triangular smoothing along the edges

$$f(t) = \begin{cases} \frac{1}{t_0}(t - t_{\mathrm{in}}), & t_{\mathrm{in}} \le t < t_{\mathrm{in}} + t_0 \\ 1, & t_{\mathrm{in}} + t_0 \le t \le t_{\mathrm{off}} - t_0 \\ \frac{1}{t_0}(t_{\mathrm{off}} - t), & t_{\mathrm{off}} - t_0 < t \le t_{\mathrm{off}}. \end{cases} \tag{2}$$

Here the duration of the effect $\tau = t_{\mathrm{off}} - t_{\mathrm{in}} - 2t_0$ is in the sub-nanosecond range, and the time t_0 is responsible for the smooth change in the pulse amplitude.

In Sec. 2.2, we will return to the details of the Hamiltonian (1) and present the results of considering a more realistic qubit model that are based on a rigorous analysis of the Hamiltonian of a three-Josephson-junction loop.

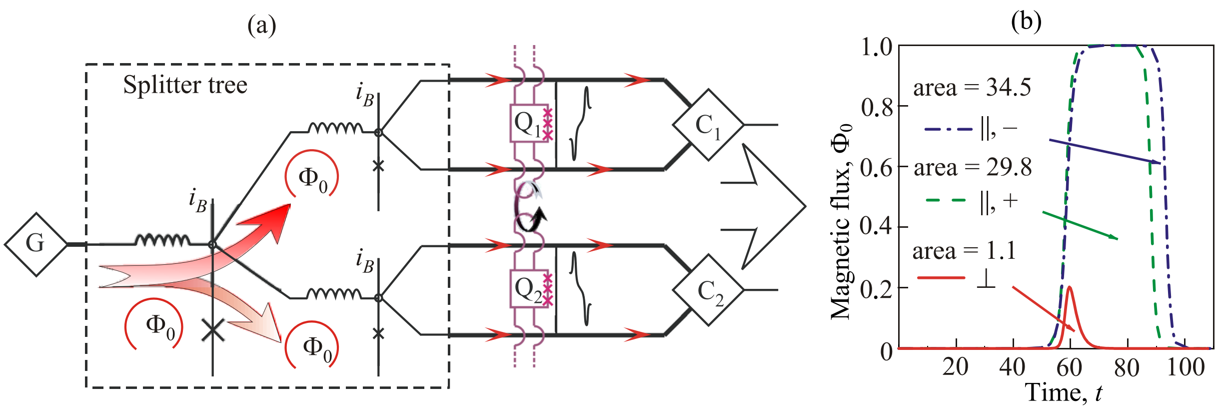

Fig. 1. (a) A sketch of the readout circuit based on a symmetric ballistic fluxon detector for a system of N qubits (Q). (b) The magnetic flux acting on the qubit as a function of the normalized time of ballistic fluxon interaction. Dashed and dash-dotted lines show the dependences for different polarities of the qubit magnetic flux for an asymmetric detector. The red solid line shows the dependence of the magnetic flux of the inverse effect in the symmetrized scheme [10].

In general the process of destroying the coherent state of the qubit will be considered as the interaction of the artificial atom and the bosonic reservoir containing a large number of degrees of freedom. In this case, the Hamiltonian of the system will look like

$$H_s = H + \sum_q \omega_q b_q^+ b_q + F_z \sigma_z + F_x \sigma_x, \quad (3)$$

where the first term H is the qubit Hamiltonian, defined by Eq. (1); the second term is the Hamiltonian of the bosonic reservoir, where b_q and b_q^+ are the boson creation and annihilation operators and ω_q is the frequency of a boson with angular momentum q; the last two terms are responsible for the interaction of the qubit and the bosonic reservoir, and $\boldsymbol{\sigma} = \{\sigma_x, \sigma_y, \sigma_z\}$ is the set of Pauli matrices. The Hermitian reservoir operators F_z, F_x, which are responsible for the longitudinal and transverse relaxation of the system, can be represented as a linear combination

$$F_{z,x} = \frac{1}{\sqrt{V}} \left(\sum_q g_{z,x}(q) b_q + \sum_q g_{z,x}^+(q) b_q^+ \right),$$

wherein $g_{z,x}(q)$ are the coupling constants, V is the system volume. The statistical properties of the reservoir operators F_z, F_x are determined by the correlation functions $K(t-t') = \langle F_{z,x}(t) F_{z,x}^+(t') \rangle$.

A noise model with a smooth spectrum ("white noise," the spectral density of which has no singularities) was chosen at the first stage of analyzing the effects a fluxon has on a qubit. In this case the thermostat correlation time is much less than the actual relaxation time of the subsystem, which makes it possible to use the Markovian approximation in deriving the equations for the subsystem of the density matrix ρ. In addition, in deriving the equation for the qubit density operator, the second order of perturbation theory was used for the interaction of the subsystem with the qubit thermostat—the Born approximation.[15] Taking into account the approximations that were made, the equation for the density matrix is written in the form

$$\frac{d\hat{\rho}}{dt}(t, \hat{\rho}(t)) = \frac{i}{\hbar}\left[\hat{\rho}(t), \hat{H}(t)\right] + \frac{\Gamma_f}{2}(\hat{\sigma}_z \hat{\rho}(t) \hat{\sigma}_z - \hat{\rho}(t)) + \frac{\Gamma_e}{2}(2\hat{\sigma}_- \hat{\rho}(t) \hat{\sigma}_+ - \hat{\sigma}_+ \hat{\sigma}_- \hat{\rho}(t) - \hat{\rho}(t) \hat{\sigma}_+ \hat{\sigma}_-), \quad (4)$$

wherein the velocity Γ_f characterizes the dephasing process with the characteristic time $T_f = 1/\Gamma_f$, the parameter Γ_e correlates to the energy relaxation rate ($T_e = 1/\Gamma_e$),[14] and $\sigma_\pm = (\sigma_x \pm i\sigma_y)/2$. The results of a number of experimental studies[16–18] allowed us to justifiably omit thermal excitation processes (spontaneous "uplift" due to temperature) because the probability of such processes is several orders of magnitude less than the values typical for the relaxation mechanisms being considered.

For further analysis we transform the Hamiltonian $H \to H\hbar$ and measure Δ and ε(t) in rad/s. The density matrix can be conveniently expanded in a complete set $\rho = \frac{1}{2}(I + \boldsymbol{\sigma} \cdot \mathbf{R})$, wherein I is the identity matrix, then Eq. (4) will be equivalent to the system of equations for the components of the Bloch vector $\mathbf{R} = \mathrm{Tr}\,(\boldsymbol{\sigma}\rho(t))$

$$\begin{cases} \dot{R}_x = -2\Delta R_y - 4\Gamma_f R_x - \Gamma_e R_x, \\ \dot{R}_y = 2\Delta R_x - 2\varepsilon(t) R_z - 4\Gamma_f R_y - \Gamma_e R_y, \\ \dot{R}_z = 2\varepsilon(t) R_y - 2\Gamma_e R_z - \Gamma_e. \end{cases} \quad (5)$$

The initial state corresponding to the ground state of the qubit with energy E_0 will be written in this case as

$$\mathbf{R}(t_{in}) = (0.0, -1),$$

And the population probabilities of the ground ("0" with energy E_0) and excited ("1" with energy E_1) states are written, respectively as

$$W_0(t) = \frac{1 - R_z}{2}, \quad W_1(t) = \frac{1 + R_z}{2}.$$

It should be noted that in the experiments with qubits[17,18] the mechanism of transverse relaxation (dephasing) usually substantially dominates the process of energy relaxation, i.e., $T_f \ll T_e$.

The effect a fluxon has on a qubit is determined by two parameters within the framework of the chosen model, which are A (amplitude), and τ (duration) and can be experimentally controlled to some extent, thereby changing the nature of the quantum system's evolution. Figure 2 shows the contour plot of the time evolution for the probability of the qubit transition $W_0(t)$ from the ground to the excited state with smooth scanning of the signal amplitude A, and the black dashed lines show the profile boundaries of the unipolar excitation pulse. The initial instant ($t = 0$) when the qubit is initialized (is ready in the ground state with energy E_0) corresponds to the red areas on the contour plot (Fig. 2). The state of the system is invariant up until the

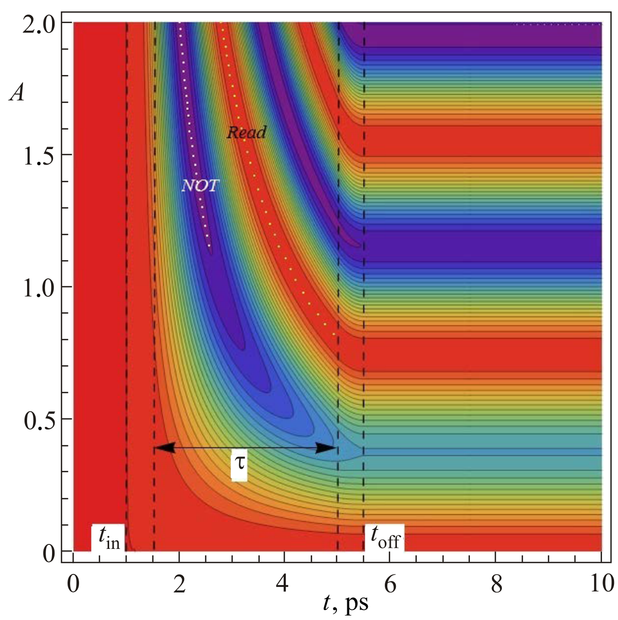

Fig. 2. The contour plot of the time evolution of population $W_0(t)$ of the qubit ground state ($\Delta/h = 1$ GHz) when scanning by the amplitude A of the acting unipolar pulse. The typical curves for the amplitude values and pulse durations, at which the reliability of the logic operation reaches 0.001%, are represented by white dots on the graph for the "*NOT*" logic operation, and as yellow dots "*Read*" for the readout operation. The noise values $\Gamma_e = 0.00001$ GHz, $\Gamma_f = 0.00005$ GHz.

moment when the excitation field is turned on $t = t_{in}$. During the exposure to a pulse with a given amplitude (horizontal sections on the contour plot) there were observable oscillations in the qubit-level populations, which looks like a pattern of alternating red and purple areas on the figure. It can be seen that as the amplitude of the exposure amplitude increases the frequency of population oscillations increases, which is also characteristic for modulated magnetic field (Rabi problem[19–21]) After exposure to the pulse has ended the qubit population is formed, which varies little and at times that are small in comparison to the phase and energy relaxation times T_f, T_e. The conducted numerical experiments have shown that it is possible to select the pulse duration for a given signal amplitude so as to:

(1) implement non-destructive readout of information with the help of a Josephson ballistic detector;
(2) carry out quantum logic operations at picosecond times.

An analysis of the calculation results has shown that the possibility of state vector flip-flop ("*NOT*" logic operation, when "0" → "1" or "1" → "0") depends on two criteria: first, the energy of the external field must be comparable to, or greater than, the distance between the levels in the qubit ($\Delta = 2\omega_{12}$, $A \geq \Delta$), and second, the pulse duration must be related to the qubit frequency as $\omega_{01}\tau \ll 1$, which was shown earlier using an analysis of the Schrödinger equation as an example.[13] Strictly speaking, two of the given conditions are not independent and in turn impose limits on the amplitude ranges and characteristic pulse durations for carrying out ultra-rapid "*NOT*" operations. For example, for a reasonable system parameter chosen for simulation purposes $\omega_{01}/2p = 0.5$ GHz, a flip-flop is possible with a minimum amplitude $A/h \sim 1.2$ GHz, corresponding to a duration of $\tau \sim 1.3$ ps. On Fig. 2 white dots show the characteristic curve on the parameter plane of the fluxon effect, on which the reliability F (*Fidelity*) of the transition from one basis state to another reaches $F = 0.9999$. Near this curve there is a region of pulse parameter (duration and amplitude) fluctuations where the operation error is no more than 2% ($F = 0.98$).

In addition, a situation in which after the unipolar exposure the system returns to its initial state ("0" → "0" or "1" → "1") is also considered, which is very interesting from the perspective of implementing a rapid non-destructive readout of quantum information. In this case there are no strict limitations to the duration or amplitude of the pulse, and at small values of the latter ($A \leq \Delta$) there are no observable oscillations between the basis levels of the qubit. The characteristic curve for the pulse parameters of operation fidelity $F = 0.9999$ is shown on Fig. 2 with yellow dots.

For a more detailed study of how the decay processes of coherent states impacts the behavior of such rapid operations, the time dependences of qubit population for different values of Γ_f were constructed (see Fig. 3) for both readout and write operations (based on the "*NOT*" operation). It is clearly visible that the increase in the rate of phase relaxation (phase failure) leads to an equilibrium population of qubit levels at $W_0(t) = 0.5$.

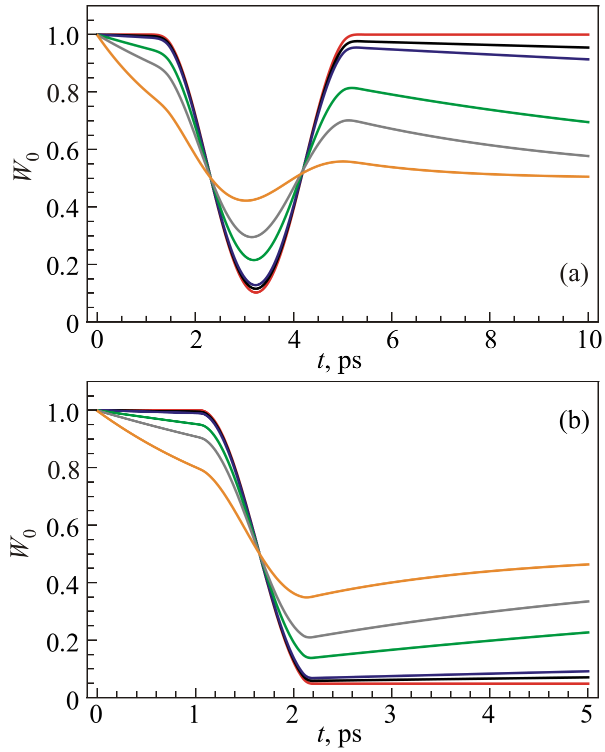

Fig. 3. Dissipative time dependences of the qubit ground state population $W_0(t)$ for information readout (a) and "*NOT*" operation (b) at different phase noise values Γ_f, GHz: 0.00005 (1); 0.0025 (2); 0.005 (3); 0.025 (4); 0.05 (5); and 0.25 (6). System parameters: $\Delta/h = 1$ GHz, $\Gamma_e = 0.00001$ GHz, $t_{in} = 1$ ps, $\delta = 2$ ps^{-1}, (a) $A/h = 0.75$ GHz and $\tau = 5$ ps; (b) $A/h = 1.3$ GHz and $\tau = 1.2$ ps.

It should be noted that in the study, the dependence of the population behavior on the smoothing factor $\delta = (t_0)^{-1}$ was also investigated. It turned out that the given parameter has no effect on the changes to the qualitative characteristics, since the pulse duration remains constant. Although, an increase in the δ parameter does cause a shift in the moment of population "collapse," the position of which corresponds to the center of the $f(t)$ function's "plateau." Note that even for triangular pulse at $\delta = \tau^{-1}$ the earlier described logic operations can be carried out.

2.2. Readout and control: analyzing the flux qubit Hamiltonian

The development of the proposed technique for analyzing the dynamics of the qubit state under the influence of a fluxon magnetic field requires the refinement of the system Hamiltonian. A rigorous calculation of the Hamiltonian matrix allowed us to demonstrate that sufficiently rapid (picosecond) operations can be implemented by also time-varying the main diagonal matrix elements of the qubit Hamiltonian, which is exactly what happens during the interaction of the well-known three-Josephson-junction (3JJ) flux qubit[22,23] and the fluxon field. An analysis of the behavior of such a system has been carried out, neglecting the inductance of the superconducting circuit and the contribution of the active resistance as per tradition, and assuming that the quasi-stationarity condition is satisfied. The matrix elements of the Hamiltonian will now be written with the conservation of dimensionality in the atomic (or spin) orthonormal basis, based on the functions that are "localized" in the vicinity of the minimum of the effective potential energy of the system:[24]

$$\psi^{r/l}(x_1 \ldots x_n, t) \equiv \psi^{r/l} = \prod_{k=1}^{n} \frac{1}{\sqrt{\sqrt{\pi} a_{x_k}^{r/l}}} \exp\left(-\left(\xi_{x_k}^{r/l}\right)^2/2\right),$$
$$\xi_{x_k}^{r/l} = \frac{x_k - (x_k)_{\min}^{r/l}}{a_{x_k}^{r/l}}. \qquad (6)$$

In generalized coordinates $(x_1 \ldots x_n)$, this basis has the form

$$\varphi_{l/r}(x_1 \ldots x_n, t) = \frac{\psi^{l/r} + c\left(\psi^l + \psi^r\right)}{\sqrt{1 - \left(\psi^l \psi^r\right)}}, \qquad (7)$$

wherein the constant c is defined as

$$c = \frac{1}{2}\left(-1 + \sqrt{\frac{1 - \left(\psi^l \psi^r\right)}{1 + \left(\psi^l \psi^r\right)}}\right), \quad \left(\psi^l \psi^r\right) = \int_O \psi^l \psi^r dx_1 \cdots dx_n. \quad (8)$$

Here $O = \{x_k\!: x_k \in (-\infty, \infty),\ k = 1 \ldots n\}$ is the domain of definition for all generalized coordinates. The designations "l" and "r" correspond to the left and right minima of the potential energy profile of the flux qubit as a function of the generalized coordinate. The wave function ψ^l is localized at the left minimum of this profile, and the function ψ^r at the right. For a physically meaningful construction of these functions the potential energy profile was approximated near each of the minima by the potential energies of the linear harmonic oscillator, which made it possible to calculate the constants $a_{x_k}^{r/l}$ from Eq. (6).

The flux qubit Hamiltonian with three Josephson junctions 1,2, and 3 that have critical currents I_C, I_C and αI_C ($\alpha = (I_C)_3/(I_C)_1 \in [0.5; 1]$), can be written as

$$\hat{H} = -\sum_{k=1}^{n} \frac{\hbar\omega_{x_k}^{r/l}}{2} \frac{\partial^2}{\partial\left(\xi_{x_k}^{r/l}\right)^2} + U, \qquad (9)$$

where the precise expression for the potential energy profile looks like

$$U(x_1 \ldots x_n, t) = E_J(2 + \alpha - 2\cos\theta\cos\varphi + \alpha\cos(2\pi f_z - 2\theta)). \qquad (10)$$

Here the generalized coordinates are expressed in terms of the Josephson phases as $\theta = \frac{\varphi_1 + \varphi_2}{2} = x_1$ and $\varphi = \frac{\varphi_1 - \varphi_2}{2} = x_2$. With the chosen parameters, the magnetic flux through the superconducting contour Φ_z can be assumed to be a given for any moment of time, such that the condition $\varphi_1 + \varphi_2 + \varphi_3 = 2\pi\ (f_z + 1/2)$, $f_z \equiv \Phi_z/\Phi_0 - 1/2$, $|f_z| \ll 1$ is valid. In the expression for the Hamiltonian, the variables $\xi_\theta^{r/l} = \frac{\theta - \theta_{\min}^{r/l}}{a_\theta^{r/l}}$ and $\xi_\varphi^{r/l} = \frac{\varphi - \varphi_{\min}^{r/l}}{a_\varphi^{r/l}}$, were used, for which $\theta_{\min}^{r/l} = \pm\theta^* + 2\pi f_z \frac{2\alpha^2 - 1}{4\alpha^2 - 1}$, $\theta^* = \arccos\frac{1}{2\alpha}$, $\varphi_{\min}^{r/l} = 0$. At the same time the constants from Eq. (6) were determined from the general formulas for the harmonic oscillator $a_\theta^{r/l} = \sqrt{\frac{\hbar}{M_\theta \omega_\theta^{r/l}}}$, $a_\varphi^{r/l} = \sqrt{\frac{\hbar}{M_\varphi \omega_\varphi^{r/l}}}$. At $|f_z| \ll 1$ we can show that $M_\theta = 2M\ (1 + 2\alpha)$, $M_\varphi = 2M$, $M = \left(\frac{\hbar}{2e}\right)^2 C$. Introducing the notation $s = E_J/E_C$ for the ratio of the Josephson and charge energies for the Josephson junctions 1 and 2, the characteristic frequencies of the approximating harmonic profile of the potential energy can be expressed as

$$\hbar\omega_\theta^{r/l} = E_J \sqrt{\frac{2\alpha - 1}{s\alpha}} \left(1 \mp \pi f_z \frac{2\alpha^2 + 1}{(4\alpha^2 - 1)^{3/2}}\right), \qquad (11)$$

$$\hbar\omega_\varphi^{r/l} = \frac{E_J}{\sqrt{s\alpha}} \left(1 \mp \pi f_z \frac{2\alpha^2 - 1}{\sqrt{4\alpha^2 - 1}}\right). \qquad (12)$$

The two-well profile of the potential energy of the 3JJ qubit, U, exists only if the condition $|f_z| \ll 1$, which is mentioned above, is fulfilled, and at values $|f_z| \approx 0.07$ ($\alpha = 0.8$) it disappears. Using the Hamiltonian operator (9) and the orthonormal basis (7), it is necessary to find the exact expression for the Hamiltonian matrix in this basis, which was done in Ref. 24. Calculating the kinetic and potential energies separately $\tilde{H}_{ij} = \tilde{T}_{ij} + \tilde{V}_{ij}, i, j = 1, 2$, it is possible to introduce a number of notations that allow to write the matrix of the Hamiltonian in an explicit form

$$c_\theta = a_\theta^r / a_\theta^l, \quad c_\varphi = a_\varphi^r / a_\varphi^l, \quad z^{l/r} = \frac{2\pi f_z}{4\alpha^2 - 1} \pm 2\theta^*,$$
$$z_1 = a_\theta^r \sqrt{\frac{2}{c_\theta^2 + 1}}, \quad z_2 = \frac{\theta_{\min}^r + c_\theta^2 \theta_{\min}^l}{c_\theta^2 + 1}, \quad z_3 = a_\varphi^r \sqrt{\frac{2}{c_\phi^2 + 1}},$$
$$z_4 = 2\pi f_z + \frac{2c_\theta^2\left(\theta_\varphi^r - \theta_{\min}^l\right)}{c_\theta^2 + 1} - 2\theta_{\min}^r,$$
$$D = \exp\left(\sum_{k=1}^{n}\left(-\frac{\left((x_k)_{\min}^r - (x_k)_{\min}^l\right)^2}{2\left(\left(a_{x_k}^r\right)^2 + \left(a_{x_k}^l\right)^2\right)}\right)\right) \sqrt{\prod_{k=1}^{n} \frac{c_{x_k}}{c_{x_k}^2 + 1}}.$$

After this, the matrix elements of the Hamiltonian of the 3JJ qubit in the non-orthonormal (meaning, auxiliary) basis (6) assume the form

$$\tilde{T}_{11} = \frac{\hbar\omega_\theta^l}{4} + \frac{\hbar\omega_\varphi^l}{4}; \quad \tilde{T}_{22} = \frac{\hbar\omega_\theta^r}{4} + \frac{\hbar\omega_\varphi^r}{4}, \qquad (13)$$

$$\tilde{T}_{12} = \tilde{T}_{21} = D\left(\frac{\hbar\omega_\theta^r c_\theta^2}{c_\theta^2 + 1}\left(1 - \frac{\left(\theta_{\min}^r - \theta_{\min}^l\right)^2}{\left(a_\theta^l\right)^2 + \left(a_\theta^r\right)^2}\right) + \frac{\hbar\omega_\varphi^r c_\varphi^2}{c_\varphi^2 + 1}\right), \qquad (14)$$

$$\tilde{V}_{11/22} = E_J\left(2 + \alpha - \frac{1}{2}\cos\theta_{\min}^{l/r} \tilde{f}\left(a_\theta^{l/r}\right) \tilde{f}\left(a_\varphi^{l/r}\right) + \frac{\alpha}{2}\cos z^{l/r} \tilde{f}\left(2a_\theta^{l/r}\right)\right), \qquad (15)$$

$$\tilde{V}_{12} = \tilde{V}_{21} = E_J D\left(4 + 2\alpha - \cos z_2 \tilde{f}(z_1) \tilde{f}(z_3) + \alpha\cos z_5 \tilde{f}(-2z_1)\right). \qquad (16)$$

In order to transition from the quantities (13)–(16) calculated in the basis of Eq. (6) to quantities calculated in the basis of Eq. (7) the following formula must be used

$$\begin{cases} H_{11/12} = \left(\tilde{H}_{11/22}(1+c)^2 + 2c(c+1)\tilde{H}_{12} + c^2\tilde{H}_{22/11}\right)/\left(1-\left(\psi^l\psi^r\right)\right) \\ H_{12} = H_{21} = \left(\tilde{H}_{12}(2c^2+2c+1) + \left(\tilde{H}_{11}+\tilde{H}_{22}\right)(c^2+c)\right)/\left(1-\left(\psi^l\psi^r\right)\right). \end{cases} \quad (17)$$

We can show that the difference between the diagonal matrix elements H_{22}–H_{11} is proportional to the normalized magnetic flux f_z and equal to zero at the degeneracy point (for the parameters in Fig. 4(a) it is approximately equal to $H_{22}–H_{11} \approx 2f_z 7.028 \times 10^{-17}$ erg). It is also interesting that according to the calculation data, with changes to f_z the value H_{12} is practically constant and proportional to D, moreover $D \ll 1$. As a result, when the parameters α and s that are given by the flux qubit topology increase, the minor diagonal matrix elements H_{12} and H_{21} exponentially tend toward zero, whereas changes to the other elements of the Hamiltonian occur much more smoothly.

Numerical analysis of the dynamics of the 3JJ flux qubit state based on the Bloch equation (the Runge-Kutta fourth-order method was used) demonstrated that the above-discussed "*NOT*" logic operation can be implemented at picosecond times by exposing the qubit to the SFQ pulse [Fig. 4(a)]. The probability of finding a system in the stationary state "0" or "1" was determined from the matrix formula

$$W_j = \left(\left(c_1^j\right)^* \left(c_2^j\right)^*\right)\begin{pmatrix}\rho_{11} & \rho_{12}\\ \rho_{21} & \rho_{22}\end{pmatrix}\begin{pmatrix}c_1^j\\ c_2^j\end{pmatrix}, \quad j=0;1$$

with the notations

$$\begin{pmatrix}c_1^j\\ c_2^j\end{pmatrix} = \frac{1}{\sqrt{1+|H_{21}/(E_j-H_{22})|^2}}\begin{pmatrix}1\\ \dfrac{H_{21}}{E_j-H_{22}}\end{pmatrix}, \quad j=0;1,$$

$$E_{1;0} = \frac{H_{11}+H_{22}}{2} \pm \sqrt{\left(\frac{H_{22}-H_{11}}{2}\right)^2 + |H_{12}|^2}.$$

In order to analyze the most "complicated" situation that occurs when the qubit interacts strongly with the control/readout gate,[25] the case of $\Gamma_f\,\tau \sim 1$ (here $\Gamma_f\,\tau \sim 10^{11}$ s^{-1}) was considered. The following explicit time dependence was used in the simulation

$$\Gamma_f(t) = \left\{[f_z(t)]/\left[(f_z)_{\mathrm{MAX}\forall t}\right]\right\}10^{11}\mathrm{s}^{-1}.$$

The corresponding dynamics of the system's stationary state populations are shown in Fig. 4(b) for the same control parameters and the same dependence $f_z(t)$ as in Fig. 4(a).

As can be seen from the graph, the general observations formulated in the previous section remain valid for the case when the fluxon acting on the qubit affects the asymmetry of the potential (the main diagonal elements of the Hamiltonian) and not the value of the barrier separating the minima (minor diagonal elements of the Hamiltonian, as is the case in Ref. 13; this case also corresponds to the mathematical model considered in Sec. 2.1.).

The use of the chosen explicit dependence $\Gamma_f(t)$ is justified by the fact that the decoherence value must be proportional to the value of the given signal $f_z(t)$. In the case of a 3JJ qubit this argument is not entirely correct, since in this instance, aside from $f_z(t)$, the contour of the qubit permeates the constant flux $\Phi_0/2$ that must also influence the dynamics of the system and the amount of decoherence. However, using a π-contact[25] instead of one of the junctions in the contour of the 3JJ qubit eliminates the need to specify the flux $\Phi_0/2$. Moreover, all equations for the 3JJ qubit will also be valid for a qubit with one π-contact, if we substitute φ_1 with $\tilde{\varphi}_1 = \varphi_1 - \pi$. Only the equation $\varphi_1 + \varphi_2 + \varphi_3 = 2\pi\,(f_z + 1/2)$ will change: in its right side, the term $1/2$ disappears.

2.3. The Bloch and Landau-Lifshitz-Gilbert equations: the equivalence conditions

Before proceeding to the analysis of the qubit parameters that are optimal for the implementation of operations

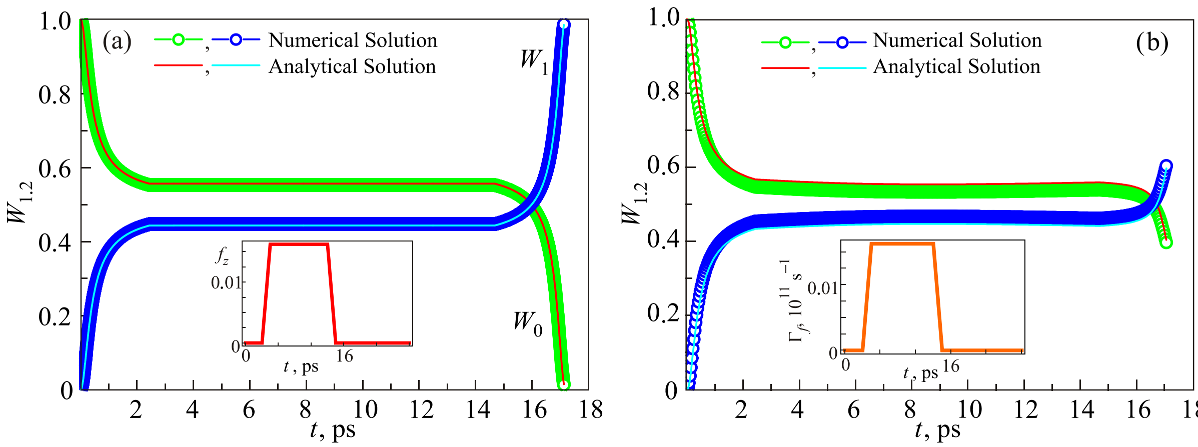

Fig. 4. (a) Simulation of the "*NOT*" operation over the 3JJ flux qubit based on the Block equation: transferring the 3JJ qubit from the ground to the first excited state without taking into account the processes of decoherence ($\tau = 17.1$ ps, $E_J = 1.72 \times 10^{-15}$ erg, $C = 1.87 \times 10^{-15}$ F, $I_C = 525$ nA, $\alpha = 0.8$, $E_J/E_C = 6.25$, $f_{z\mathrm{MAX}} = 0.0157$, $\Gamma_f = \Gamma_e = 0$). (b) Dynamics of the 3JJ qubit with the same control parameters and in the presence of a strong phase decoherence [$(\Gamma f)_{\mathrm{MAX}}=10^{11}$ s^{-1}, $\Gamma_e=0$]. The time dependences of the normalized magnetic flux that controls the qubit dynamics (a) and the phase decoherence parameter (b) are shown on the insets.

relevant to this article, it is necessary to devote some attention to the following clear qualitative analogy. Combinations of the Hamiltonian matrix elements can be conveniently examined as a magnetic field acting on the magnetic moment, with the z-component (proportional to $(H_{22}–H_{11})/2$ and f_z) rotating the Bloch vector (magnetic moment) and the x-component (proportional to H_{12}) impacting the amplitude of the rotation. The Landau-Lifshitz-Gilbert (LLG)[27] equation, which describes the dynamics of the classical magnetic moment in a magnetic field in the presence of coupling with the environment ("relaxation") can be written as

$$\frac{d\mathbf{m}}{dt} = g[\mathbf{m}\times\mathbf{H}] - \frac{\Pi|g|}{|\mathbf{m}|}[\mathbf{m}\times[\mathbf{m}\times\mathbf{H}]],\ \ \Pi>0,\ \ g=\frac{\gamma}{1+\Pi^2}. \tag{18}$$

Here γ is the gyromagnetic ratio and Π is the Gilbert relaxation parameter.

Let us formulate the simplifications that must be applied to the Bloch and LLG equations so that they become equivalent up to notation. Without taking into account the processes of decoherence of the states, only the first term is conserved on the right side of Eq. (18) (in this case we are talking about a precession equation). The quantum analogue of the magnetic moment vector $\mathbf{m}(t)$ is the Bloch vector $\mathbf{R}(t) = R_x(t)\mathbf{n_x} + R_y(t)\mathbf{n_y} + R_z(t)\mathbf{n_z}$, which is related to the quantum state given by the density matrix, using the relations $R_x(t) = \rho_{12}(t) + \rho_{21}(t)$, $R_y(t) = i(\rho_{12}(t) - \rho_{21}(t))$, $R_z(t) = \rho_{11}(t) - \rho_{22}(t)$. It can be seen from the Bloch equation (4) that the dynamics of the qubit state do not change if the Hamiltonian matrix is rewritten as

$$\hat{H}(t) = \begin{pmatrix} -(H_{22}-H_{11}/2) & H_{12} \\ H_{12}^{*} & -(H_{22}-H_{11})/2 \end{pmatrix}$$

and then

$$\begin{cases} \dfrac{dR_x(t)}{dt} = \omega_0(t)R_y(t) - \big(\Gamma_f + \Gamma_e/2\big)R_x(t), \omega_0(t) = (H_{22}(t) - H_{11}(t))/\hbar \\ \dfrac{dR_y(t)}{dt} = -\omega_0(t)R_x(t) - \omega_{\text{rot}}(t)R_z(t) - \big(\Gamma_f + \Gamma_e/2\big)R_y(t), \omega_{\text{rot}}(t) = 2H_{12}(t)/\hbar \\ \dfrac{dR_z(t)}{dt} = \omega_{\text{rot}}(t)R_y(t) - \Gamma_e(1 + R_z(t)). \end{cases} \tag{19}$$

Now, we can clearly see the complete analogy between the Bloch and the LLG equations without having to account for the decoherence processes. In fact, if we introduce the effective magnetic field $\gamma\mathbf{H}(t) = -\omega_{\text{rot}}(t)\mathbf{n}_x + \omega_0(t)\mathbf{n}_z \equiv \equiv \gamma\mathbf{H}_x(t) + \gamma\,\mathbf{H}_z(t)$ and identify the vectors $\mathbf{m}(t)$ and $\mathbf{R}(t)$, then the previous equation for $\Gamma_f = 0$, $\Gamma_e = 0$ reduces to the form

$$\frac{d\mathbf{m}(t)}{dt} = \gamma[\mathbf{m}(t)\times\mathbf{H}(t)], \tag{20}$$

which coincides with the well-known precession equation [Eq. (18) at $\Pi = 0$].

The dynamics of the Bloch vector components when performing the "*NOT*" logic operation are shown in Fig. 5(a) and clearly illustrate the analogy discussed above.[13] It can be seen that finding the system in the ground stationary state corresponds to the case when the Bloch vector $\mathbf{R}(t)$ is directed along the Ox ($R_x(t)$=1) axis, and the occurrence of the first excited stationary state corresponds to the case when $\mathbf{R}(t)$ is directed against the said axis ($R_x(t) = -1$).

In the considered process ($\Pi = 0$, $\Gamma_f = 0$ and $\Gamma_e = 0$) the effective magnetic field $\gamma\mathbf{H}_z(t) = \omega_0(t)\mathbf{n}_z$ $f_z(t) \neq 0$ (and, accordingly $H_{11}(t) \neq H_{22}(t)$). In this time interval, when the qubit interacts with the fluxon $|\omega_0(t)| \gg |\omega_{\text{rot}}(t)|$, $|\mathbf{H}_z(t)| \gg |\mathbf{H}_x(t)|$ and $\gamma\mathbf{H}(t) \approx \gamma\mathbf{H}_z(t)$, and therefore the Bloch vector rotates by π radian around the Oz axis, and it is in this way that the $\mathbf{H}_z(t)$ field allows for the "*NOT*" operation to be performed. At the same time the x-projection of the $R_x(t)$ Bloch vector changes signs, the y-projection of $R_y(t)$ vector is equal to zero at the beginning and at the end of the process, and the z-component of $R_z(t)$ is always approximately equal to zero and does not change, which is as it should be in the precession around the Oz axis. If after exposure the system remains at the point of degeneracy ($f_z(t) = 0$), then the condition $\omega_0(t) = 0$ will be fulfilled for the system, and therefore in accordance with the first of Eq. (19) the value $R_x(t)$ will be constant, and the system will not leave the stationary state until the decoherence mechanisms of the qubit states manifest themselves. A numerical calculation has shown that the growth of the field $\mathbf{H}_x(t)$ can lead to a "decrease" in the precession amplitude, described above, and is therefore undesirable.

Now consider a situation in which the found analogy is violated. Given non-dissipative dynamics the Bloch vector has a unit length and ends at the surface of the Bloch sphere. The situation changes in the presence of a phase (and/or energy) "decoherence." The corresponding dynamics of the Bloch vector components are shown in Fig. 5(b) at times of about 300 ps, which is when the decoherence processes manifest themselves. The state of the system in the process of dynamics becomes mixed, and the Bloch vector becomes less than unit length. If an attempt is made at extending the analogy to Eq. (18) while accounting for all the terms, than it can be shown that the length of the classical magnetic moment vector will also be constant for $\Pi \neq 0$ while the length of the quantum Bloch vector decreases. In addition, it can be shown that over the course of the dynamics described

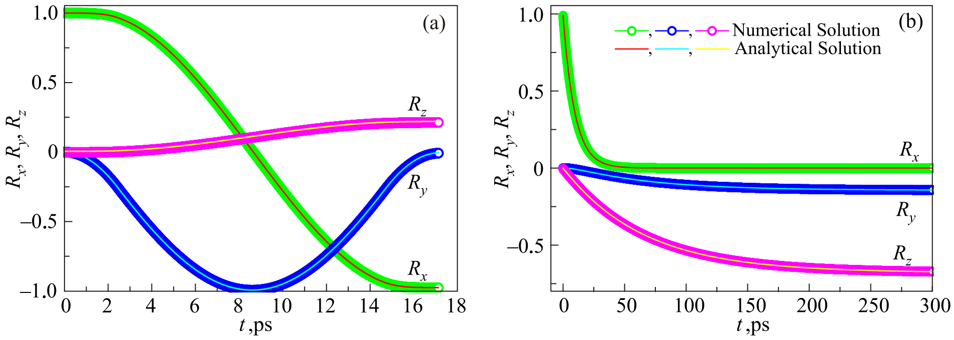

Fig. 5. The components of the Bloch vector of the 3JJ qubit ($E_J = 1.72 \times 10^{-15}$ erg, $C = 1.87 \times 10^{-15}$ F, I_C = 525 nA, $\alpha = 0.8$, $E_J/E_C = 6.25$) as functions of time (a) when performing the "*NOT*" logic operation without accounting for the processes of state decoherence (τ = 17.1 ps, $f_{z\mathrm{MAX}}$ = 0.0157, $\Gamma_f = \Gamma_e = 0$); (b) at f_z=0 and given the presence of strong coupling with control and readout circuits (τ = 300 ps, $\Gamma_f \sim 10^{11}$ s^{-1}, $\Gamma_e \sim 10^{10}$ s^{-1}).

by Eq. (18), for a field with a constant direction $\mathbf{H}(t)$ and $\Pi = \mathrm{const} \neq 0$, the vector $\mathbf{m}(t)$ in the process of its dynamics eventually turns out to be directed along the vector $\mathbf{H}(t)$. Concerning Fig. 5(b), in this case the dynamics of the 3JJ qubit state were studied at the point of degeneracy, when in the effective magnetic field only the term $\gamma\mathbf{H}_x(t)$ was non-zero: here, under the influence of the phase and energy relaxation the Bloch vector acquires a nonzero z-projection $R_z(t)$ and a non-zero y-projection $R_y(t)$, while its x-projection $R_x(t)$ turns out to be equal to zero. Thus, unlike the classical LLG equation, the dynamics of the quantum Bloch vector in the presence of coupling with the environment reduces to its reorientation perpendicular to the effective magnetic field, for a traditional flux qubit at reasonable system parameters.

2.4. Readout and control: optimizaiton of the qubit parameters

In order to study the possibilities for an optimal execution of a "*NOT*" logic operation within the framework of a sufficiently realistic model for a 3JJ flux qubit, and apply the recently obtained clear quantum-classical analogy, we consider the constant and negligibly small "decoherence parameters": $\Gamma_f = 10^7$ s^{-1}, $\Gamma_e = 10^6$ s^{-1}. In the new notation the conditions for carrying out such an operation can be formulated as the requirement that $|\omega_{\mathrm{rot}}| \ll |\omega_0|$ (or $|\omega_0/\omega_{\mathrm{rot}}| \equiv |(H_{22}–H_{11})/(2H_{12})| \gg 1$) for $f_z \neq 0$, which allows us to neglect in Eq. (19) the terms containing ω_{rot}. For this case the Bloch equation is solved analytically:

$$\begin{cases} R_x(t) = \exp\left(-\left(\Gamma_f + \Gamma_e/2\right)t\right)\left(R_x(0)\cos\lambda(t) + R_y(0)\sin\lambda(t)\right), \lambda(t) = \int\limits_0^t \omega_0(t')dt' \\ R_y(t) = \exp\left(-\left(\Gamma_f + \Gamma_e/2\right)t\right)\left(-R_x(0)\sin\lambda(t) + R_y(0)\cos\lambda(t)\right) \\ R_z(t) = (1 + R_z(0))\exp\left(-\Gamma_e t\right) - 1. \end{cases} \tag{21}$$

For the initial condition $\mathbf{R}(0)=\{1,0,0\}$ given an insignificant decoherence $R_x(t)=\cos\lambda(t)$, so that the "*NOT*" operation can be implemented by the Bloch vector rotation around the Oz axis with an angular velocity ω_0 if $|\omega_{\mathrm{rot}}| \ll \omega_0$ and the solution to Eq. (21) is applicable. The duration of the interaction between the fluxon and the qubit, determined by the rate of fluxon motion, must in this case be selected such that the condition $\lambda(t) = \pi$ is fulfilled. However if the condition $|\omega_{\mathrm{rot}}| \ll |\omega_0|$ is violated, a rotation around the Ox axis with a frequency ω_{rot} is superimposed on this rotation, which decreases the "amplitude" of the main rotation and prevents the realization of the "*NOT*" operation.

Within the framework of this model we understand the dynamics of the 3JJ qubit state exposed to an external field, during which the populations of the stationary states return to initial values after interacting with the fluxon [see Fig. 6(a)], as the readout operation. By comparing this figure with Fig. 4(a) it can be seen that all other things being equal, the magnetic flux f_{z0} that is required for readout is exactly twice as large as the magnetic flux that is required for the "*NOT*" operation, if $\omega_{\mathrm{rot}}\tau \leq 1$. When $\omega_{\mathrm{rot}}\,\tau \gg 1$ the restriction on the magnitude of the inverse effect the "readout" fluxon has on the qubit can be removed [see the curve "*Read*" on Fig. 6(b)]: for sufficiently long exposure times the readout can be successfully implemented regardless of how accurately its duration is selected. The graphs in Fig. 6 were obtained under the condition that in terms of magnitude, the product of fluxon pulse duration and its amplitude is about constant, and that for readout it is twice as large as for the write operation.

In order to optimize the "*NOT*" operation implementation mode it is convenient to consider it as a change in the population of the second stationary state from zero to the value $W_{\max}$, which must lie as close as possible to one. This value, as a function of the $\omega_{\mathrm{rot}}\tau$ parameter is presented as the "*NOT*" curve on Fig. 6(b): the implementation of the "*NOT*" logic operation by the described method is possible only for $\omega_{\mathrm{rot}}\,\tau \ll 1$. Since the duration for the "*NOT*" operation is determined by the value ω_0, the conditions $|\omega_{\mathrm{rot}}| \ll |\omega_0|$ and $\omega_{\mathrm{rot}}\,\tau \ll 1$ are equivalent.

3. Conclusion

The readout and control operations over the qubit states can be implemented by exposing the qubit to a ballistic

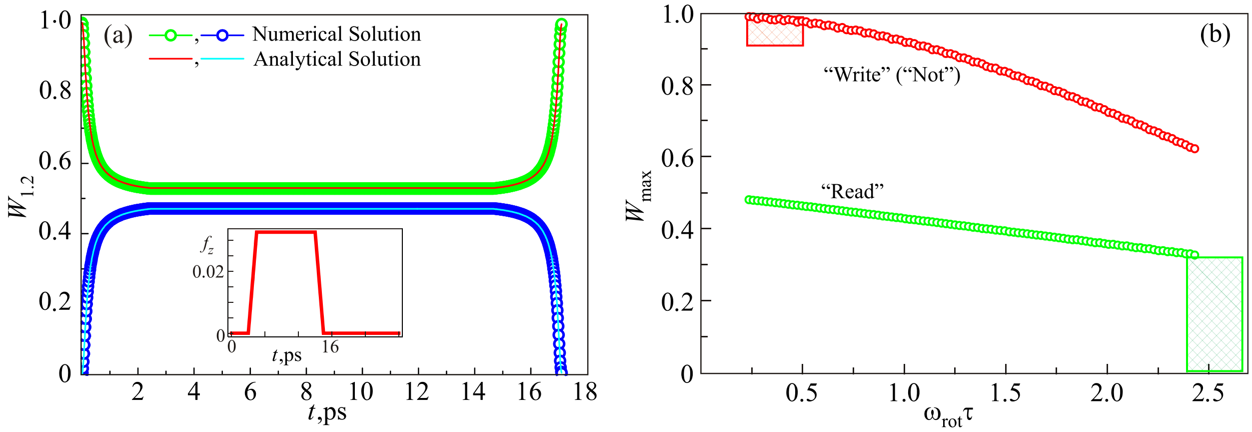

Fig. 6. (a) The dynamics of the stationary state populations of the 3JJ qubit ($E_J = 1.72 \times 10^{-15}$ erg, $C = 1.87 \times 10^{-15}$ F, $I_C = 525$ nA, $\alpha = 0.8$, $E_J/E_C = 6.25$) when implementing readout operations ($W_{max} = 0.48$, $\tau = 17.1$ ps, $f_{zMAX} = 0.0314$). (b) Red curve: the dependence of the maximum possible population of the first excited stationary state W_{max} of the 3JJ qubit on the parameter $\omega_{rot}\tau$ when performing the "*NOT*" operation. The green curve is the dependence of the maximum "span" ΔW of the level population for the readout operation. The parameters of the 3JJ qubit are the same as in (a).

fluxon, as well as to a fractional fluxon (semi-fluxon), propagating almost without energy dissipation in adiabatic superconductor logic circuits.[28–30] The specificity of the macroscopic quantum interference in such multi-element systems allows for the creation of a readout/control soliton-like wave of the required type of currents.[31,32] In addition, here it is possible to vary the rate of fluxon (semi-fluxon) propagation along the Josephson transmission line (by changing the supply current, for example), directly over the course of the experiment and within a fairly large range, thus controlling the duration of the qubit-fluxon interaction. The effective control over the population of the qubit stationary state is possible only if certain conditions for the duration and matrix elements of the qubit Hamiltonian are fulfilled: $\omega_{rot} \ll \omega_0$, $\omega_{rot}\ \tau \ll 1$. As demonstrated by the performed calculations, for the three-Josephson-junction flux qubit this condition is well-satisfied, if the condition for the relation between the Josephson and Coulomb energy of the elements $s = E_J/E_C{:}s \gg 1$ is also satisfied; otherwise the value of ω_{rot} increases sharply. On a practical level this means that there is no use in utilizing a value of s that is less than 5, which does not present any technical difficulties as of today. By substantially increasing the effective duration of the fluxon effect on the qubit, we can transition to the readout mode, thus obtaining information about the state of the artificial quantum system and creating a relatively weak "perturbation" in the latter.

The work was supported by the Ministry of Education and Science of the Russian Federation, the Grant of the President of the Russian Federation No. 5813.2016.2 and Grant No. 14.Y26.31.0007 (Secs. 1 and 2.2), as well as the RFBR Grant Nos. 16-29-09515 ofi_m theme (Secs. 2.3 and 2.4), 16-57-51045 NIF-a, 16-07-01012-a (Sec. 2.1), and within the framework of executing the project part of the state initiative of the Ministry of Education and Science of the Russian Federation No. 3.3026.2017/PC (Sec. 2.1).

[a)]Email: nvklenov@gmail.com

[1]S. K. Tolpygo, Fiz. Nizk. Temp. **42**, 463 (2016) [Low Temp. Phys. **42**, 361 (2016)].
[2]V. K. Kaplunenko and A. V. Ustinov, Eur. Phys. J. B **38**, 3 (2004).
[3]D. V. Averin, K. Rabenstein, and V. K. Semenov, Phys. Rev. B **73**, 094504 (2006); A. Fedorov, A. Shnirman, G. Schoen, and A. Kidiyarova-Shevchenko, *ibid.* **75**, 224504 (2007).
[4]A. Herr, A. Fedorov, A. Shnirman, E. Il'ichev, and G. Schon, Supercond. Sci. Technol. **20**, S450 (2007).
[5]L. Pankratov, A. V. Gordeeva, and L. S. Kuzmin, Phys. Rev. Lett. **109**, 087003 (2012).
[6]K. G. Fedorov, A. V. Shcherbakova, R. Scheafer, and A. V. Ustinov, Appl. Phys. Lett. **102**, 132602 (2013).
[7]I. I. Soloviev, N. V. Klenov, A. L. Pankratov, E. Il'ichev, and L. S. Kuzmin, Phys. Rev. E **87**, 060901(R) (2013).
[8]K. G. Fedorov, A. V. Shcherbakova, M. J. Wolf, D. Beckmann, and A. V. Ustinov, Phys. Rev. Lett. **112**, 160502 (2014).
[9]I. Soloviev, N. V. Klenov, A. L. Pankratov, L. S. Revin, E. Il'ichev, and L. S. Kuzmin, Phys. Rev. B **92**, 014516 (2015).
[10]I. I. Soloviev, N. V. Klenov, S. V. Bakurskiy, A. L. Pankratov, and L. S. Kuzmin, Appl. Phys. Lett. **105**, 202602 (2014).
[11]N. Takeuchi, D. Ozawa, Y. Yamanashi, and N. Yoshikawa, Physica C **470**, 1550 (2010).
[12]R. McDermott and M. G. Vavilov, Phys. Rev. Appl. **2**, 014007 (2014).
[13]N. V. Klenov, A. V. Kuznetsov, I. I. Soloviev, S. V. Bakurski, and O. V. Tikhonova, Beilstein J. Nanotechnol. **6**, 1946 (2015).
[14]A. N. Omelyanchuk, E. V. Il'ichev, and S. N. Shevchenko, *Quantum Coherent Phenomena in Josephson Qubits* (Naukova Dumka, Kiev, 2013).
[15]M. O. Scully and M. S. Zubairy, *Quantum Optics* (Cambridge University Press, Cambridge, 1997).
[16]D. M. Berns, W. D. Oliver, S. O. Valenzuela, A. V. Shytov, K. K. Berggren, L. S. Levitov, and T. P. Orlando, Phys. Rev. Lett. **97**, 150502 (2006).
[17]D. M. Berns, M. S. Rudner, S. O. Valenzuela, K. K. Berggren, W. D. Oliver, L. S. Levitov, and T. P. Orlando, Nature **455**, 51 (2008).
[18]J. Bylander, M. S. Rudner, A. V. Shytov, S. O. Valenzuela, D. M. Berns, K. K. Berggren, L. S. Levitov, and W. D. Oliver, Phys. Rev. B. **80**, 220506 (R) (2009).
[19]C. H. van der Wal1, A. C. J. ter Haar, F. K. Wilhelm, R. N. Schouten, C. J. P. M. Harmans, T. P. Orlando, S. Lloyd, and J. E. Mooij, Science **290**, 773 (2000).
[20]Ya. S. Greenberg, A. Izmalkov, M. Grajcar, E. Il'ichev, W. Krech, H.-G. Meyer, M. H. S. Amin, and A. M. van den Brink, Phys. Rev. B **66**, 214525 (2002).
[21]I. Chiorescu, Y. Nakamura, C. J. P. M. Harmans, and J. E. Mooij, Science **299**, 1869 (2003).
[22]J. E. Mooij, T. P. Orlando, L. Levitov, Lin Tian, C. H. van der Wal, and Seth Lloyd, Science **285**, 1036 (1999).
[23]F. Yan, S. Gustavsson, A. Kamal, J. Birenbaum, A. P. Sears, D. Hover, T. J. Gudmundsen, D. Rosenberg, G. Samach, S. Weber, J. L. Yoder, T. P. Orlando, J. Clarke, A. J. Kerman, and W. D. Oliver, Nat. Commun. **7**, 12964 (2016).
[24]A. V. Kuznetsov and N. V. Klenov, Moscow Univ. Phys. Bull. (to be published).
[25]N. V. Klenov, A. V. Sharafiev, S. V. Bakurskiy, and V. K. Kornev, IEEE Trans. Appl. Supercond. **21**, 864 (2011).
[26]N. V. Klenov, N. G. Pugach, A. V. Sharafiev, S. V. Bakurskiy, and V. K. Kornev, Phys. Solid State **52**, 2246 (2010).

[27]P. J. D. Crowley and A. G. Green, Phys. Rev. A **94**, 062106 (2016).
[28]V. K. Semenov and D. V. Averin, IEEE Trans. Appl. Supercond. **13**, 960 (2003).
[29]N. Takeuchi, D. Ozawa, Y. Yamanashi, and N. Yoshikawa, Supercond. Sci. Technol. **26**, 035010 (2013).
[30]Jie Ren and V. K. Semenov, IEEE Trans. Appl. Supercond. **21**, 780 (2011).
[31]V. K. Kornev, I. I. Soloviev, N. V. Klenov, and O. A. Mukhanov, IEEE Trans. Appl. Supercond. **17**, 569 (2007).
[32]A. E. Schegolev, N. V. Klenov, I. I. Soloviev, and M. V. Tereshonok, Beilstein J. Nanotechnol. **7**, 1397 (2016).

Translated by A. Bronskaya